Journal of Applied Sciences and Nanotechnology, Vol. 2, No. 3 (2022)

Journal of Applied Sciences and Nanotechnology

Journal homepage: https://jasn.uotechnology.edu.iq/

Spectroscopic and Structural Analysis of Aluminum Bulk and Nanoparticles: A Comparative Study

Hajir M. Fadhil*, Khaleel I. Hassoon, Hyder A. Salih

Department of Applied Sciences, University of Technology – Iraq

Article information

Article history:
Received: October, 19, 2021
Accepted: March, 25, 2022
Available online: September, 10, 2022

Keywords:
LIBS,
Optical Emission Spectroscopy,
X-Ray Diffraction,
Scanning electron microscopy

Corresponding Author:
Hajir M. Fadhil
as.18.35@grad.uotechnology.edu.iq

Abstract

In the present work, Laser Induced Breakdown Spectroscopy (LIBS) has been utilized to investigate two forms of aluminum samples, namely Al in the form of the nanoparticles (NPs) and a bulk (pellet). The Al target was irradiated by pulsed Nd-YAG laser with wavelength 1064 nm to produce plasma. The plasm spectrum is analyzed in the wavelength range between 250 nm and 700 nm. Some plasma parameters were calculated, including electron temperature (T_e), plasma density (n_e) and Debye length (λ_D) for different laser energies. The temperature of electrons was computed employing the Boltzmann plot technique, and the electrons density was computed utilizing the Stark broadening technique. This work aims to investigate the effect of laser energy on the plasma parameters and the influence of using two different forms of targets on these parameters. It was noted that increasing the laser energy from (400 mJ) to (700 mJ) resulted in an increase in electrons temperature from (0.52 eV) to (0.65 eV) and an increase in electron density from (57.38×10^{16} cm^{-3}) to (67×10^{16} cm^{-3}) for the nano aluminum plasma, whereas the electrons temperature increased from (0.52 eV) to (0.59 eV) and the electron density increased from (43.88×10^{16} cm^{-3}) to (55.05×10^{16} cm^{-3}) for the bulk aluminum plasma. From the obtained results, it's concluded that using identical laser energies, the electron temperature and electron density of the plasma generated from aluminum in the form of nanoparticles are greater than that generated from aluminum in the bulk form. The differences in the calculated parameters for Al NPs and Al bulk belong to their different structures and morphologies as presented via Scanning Electron Microscope (SEM) and X-ray Diffraction (XRD) methods.

DOI: 10.53293/jasn.2022.4365.1104, Department of Applied Sciences, University of Technology

1. Introduction

Laser-Induced Breakdown Spectroscopy (LIBS) is an invaluable method for detecting and characterizing materials [1]. It has been used in a broad range of environments owing to its simplicity of implementation. There are three phases of the materials of sample: Solid, Liquid and Gas, and LIBS is an appropriate approach to study the samples in any of these states [2,3]. When compared to many other methods of elemental analysis, it is

one of the simplest approaches [4]. This technique works by concentrating a high-powered laser beam on a sample to create a plasma, which is then gathered and utilized to achieve qualitative and quantitative data on the target composition [5]. The emitted radiation is measured with a suitable detection device (commonly a spectrophotometer) and is linked to the chemical analysis of the sample [6]. Spectroscopic study of plasma emission revealed a vast spectrum of particular lines from the ions, atoms and molecules into the ablation column, demonstrating its enormous potential for direct chemical analysis [7]. Laser parameters (energy, wavelength, etc.) have a significant impact on the laser-matter interaction and subsequently on the analytical capabilities [8]. LIBS has several advantages, including quick detection, safety, non-destructiveness, multi-element analysis at the same time, and no need for previous preparation, remote analysis, in-field detection, and a simple design for the field use [9-12]. The LIBS approach has been widely used in a variety of applications, including space exploration, geological surveying, archaeological inquiry, environmental monitoring, metals description, food discovery, agriculture monitoring, and industry monitoring [13]. One of LIBS disadvantages is its low sensitivity when it comes to analyze the trace elements in the materials in diverse domains with the analysis of the elements complex spectral lines, like the nuclear fuel components. Several methods for raising LIBS emission intensity to improve sensitivity have been devised [14]. Nanoparticles of noble metals have lately become the subject of research because of the exceptional high surface area to volume ratio which offers excellent catalytic, optical, and electrical characteristics, and they have unique physical features that set them apart from the rest of the solid-state (bulk) [15-17]. From the point of physics, laser-induced plasma must be quantified via measuring the electron temperature and electron density. The plasma parameters are commonly determined using optical emission spectroscopy (OES) by evaluating the emitted light [18]. The laser peak power influence on the spectral line intensities is demonstrated. There is also a report on plasma properties, including the electron temperature (T_e) and the electron density (n_e), as well as their relationships with the laser peak power. The Stark broadening equation is employed for calculating the electron density. The Boltzmann plot technique has been used to calculate the electron temperature. Is the present work aims to study the plasma spectrum, morphology and structure for two forms of aluminum samples.

2. Theoretical Methodology

One of the highly dependable methods for calculating the number of electron density is to study the Stark broadening line profile of an isolated line of either a neutral atom or a single charged ion. The number of electron density (N_e) is proportional to the Full Width at Half Maximum (FWHM) of the Stark broadening lines given via the subsequent equation:

$$\Delta\lambda_{1/2} = 2\omega\left(\frac{N_e}{10^{16}}\right) + 3.5A\left(\frac{N_e}{10^{16}}\right)^{(1/4)}\left(1 - BN_D^{-1/3}\right)\omega\left(\frac{N_e}{10^{16}}\right) \quad (1)$$

Where, N_e is the number of electron density, A is the ion broadening parameter, ω is the electron impact width parameter, and N_D is the particles number within the Debye sphere. In Eq. 1, the initial term indicates the broadening caused by electron contribution, whereas the ion broadening is the second term. Ionic broadening can be ignored because its impact is usually relatively small. Eq. (1) was used to compute the number of electron densities from the line profiles of the isolated aluminum neutral lines, but without accounting for the effects of the ion impact widening and the Doppler broadening, giving this fresh equation [19]:

$$N_e = \left(\frac{\Delta\lambda}{2\,\omega}\right)N_r \quad (2)$$

Where Δλ: The Lorentzian FWHM of line, ω: The Stark broadening parameter, N_r: The standard electron density equals (10^{16} cm^3) for the neutral atoms and (10^{17} cm^3) for the singly charged ions [20, 21].

The temperature of plasma can be computed from the emission-line intensities of Al using the Boltzmann plot technique under a presumed Local Thermodynamic Equilibrium (LTE) situation, where the electron collisions emissions are much bigger than those from the radiative methods [20].

$$\ln\left(\frac{I\,\lambda}{A\,g}\right) = \frac{E}{KT} + \ln\left(\frac{hcN}{4\pi U}\right) \quad (3)$$

Where, λ is the wavelength, A is the spectral line transition probabilities, g is the upper state statistical weight, E is the upper state energy (eV), K is the constant of Boltzmann, T is the temperature of electrons, h is the constant of Planck, c is the velocity of light, N is the state population densities, and U is the partition function [22].
Debye's plasma length is given as [23]:

$$\boldsymbol{\lambda_D = \left(\frac{\varepsilon_0 k_B T_e}{n_e e^2}\right)^{1/2}} \quad (4)$$

According to Eq. (5), the plasma frequency (ω_p) is proportional to the electron density.

$$\boldsymbol{\omega_p^2 = \frac{N_e\, e^2}{m_e\, \varepsilon_0}} \quad (5)$$

Where ε_0 denotes the free space permittivity, m_e denotes the electron mass, and e denotes the electron charge [24].

3. Experimental Procedure

3.1. Sample Preparation

One gram of aluminum powder (99% purity) was first prepared and then pressed under a pressure of 8 tons by a hydraulic piston to produce a single circular disk having the dimensions of 1.5 cm in diameter and 0.5 cm in thickness, as shown in Figure 1. XRD (SHIMADZU XRD 600C) was utilized for examining the samples' crystallite size. The apparatus employs Al nanoparticles and Al bulk as the targets of Cu-Kα radiation, λ = 1.5418 Å, and operates at (30 mA) and (40 kV). Measurements were done using a 2θ scan from 20° to 80°. A scanning electron microscope (SEM) of type FESEM (Zeiss Sigma 300- HV) was used for examing the size of particles and morphology of samples.

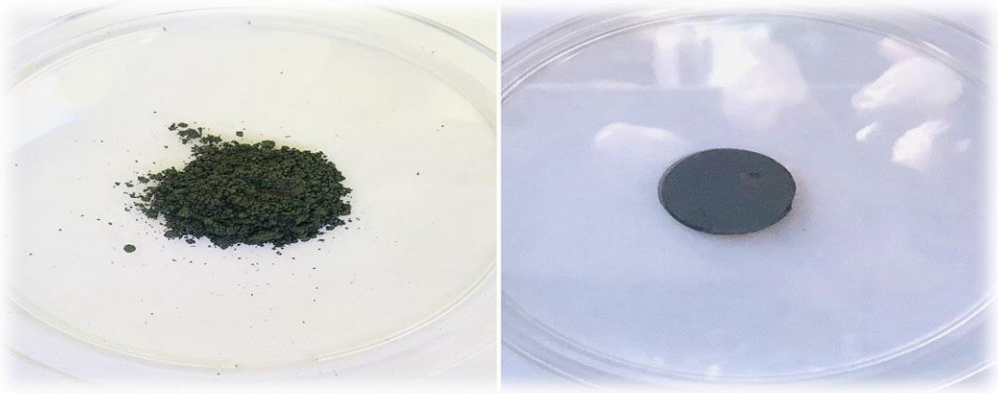

Figure 1: The shape of the aluminum material before and after pressing.

3.2. Generation of Plasma

Figure 2 depicts schematically the experimental setup of LIBS. In this experiment, Nd: YAG laser with an essential wavelength (1064 nm) was our laser source. The laser energy was set within (400-700 mJ) per pulse, (9 ns) pulse period, and rate of replication (6 Hz). A sample was targeted via laser beam at a distance of 10 cm, and an optical fiber with a photodetector was adjusted at 45° to characterize the laser-induced plasma for aluminum by using a spectrophotometer (Surwit, model S3000-UV-NIR). The data are used for the calculation of electron densities, plasma temperatures, plasma frequency, and Debye length of plasmas. The results will be compared with the standard database given by the national institute of standards and technology (NIST) [25].

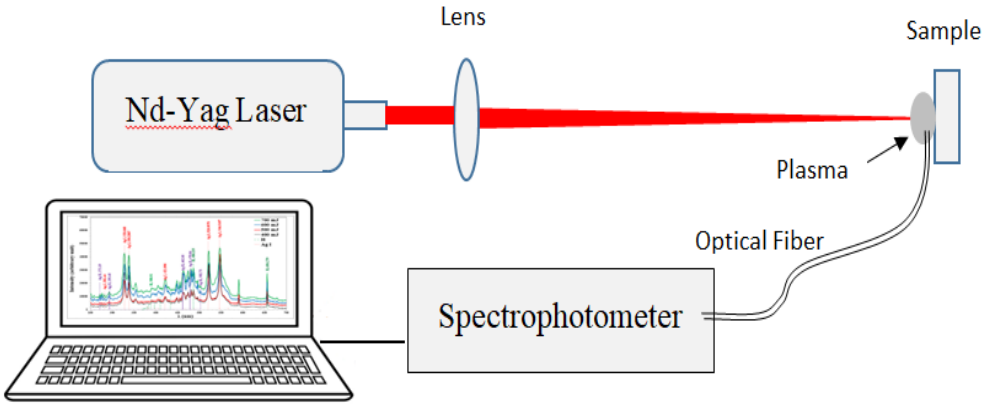

Figure 2: The schematic diagram of the experimental setup of (LIBS).

4. Results and Discussion

4.1. X-ray Diffraction (XRD)

The X-ray diffraction method is employed for determining the crystalline nature and particle size of crystalline nanomaterials [26]. To calculate the average crystal size, Debye Scherer's equation was utilized. [27]:

$$\boldsymbol{D = \frac{0.9\,\lambda}{\beta cos\Theta}} \tag{6}$$

where (D) represents the crystallite size, (λ) is the wavelength of X-ray, (β) is the FWHM of the corresponding peak, and (Θ) is the diffraction angle (in degrees). The XRD pattern of Al NPs is displayed in Figure 3a which reveals four sharp peaks (2Θ = 38.52°, 44.48°, 65.16°, and 78.36°). These peaks correspond to Miller indices of (111), (200), (220), and (311), respectively. The results are presented in Table 1. The crystalline structure of ALNPs is face-centered cubic (FCC)**.** The results are in line with the findings of a prior study of Tabari [28]. Figure 3b shows the XRD diffraction patterns for the Al bulk. This pattern has two sharp peaks. Two typical peaks for aluminum (2Θ = 65.08° and 78.2°, respectively) were identified, corresponding to Miller indices (220) and (311), respectively (Table 2). The resulting particles were found to be pure face-centered cubic aluminum. This agrees with the results reported by a previous study of Suprapedi [29].

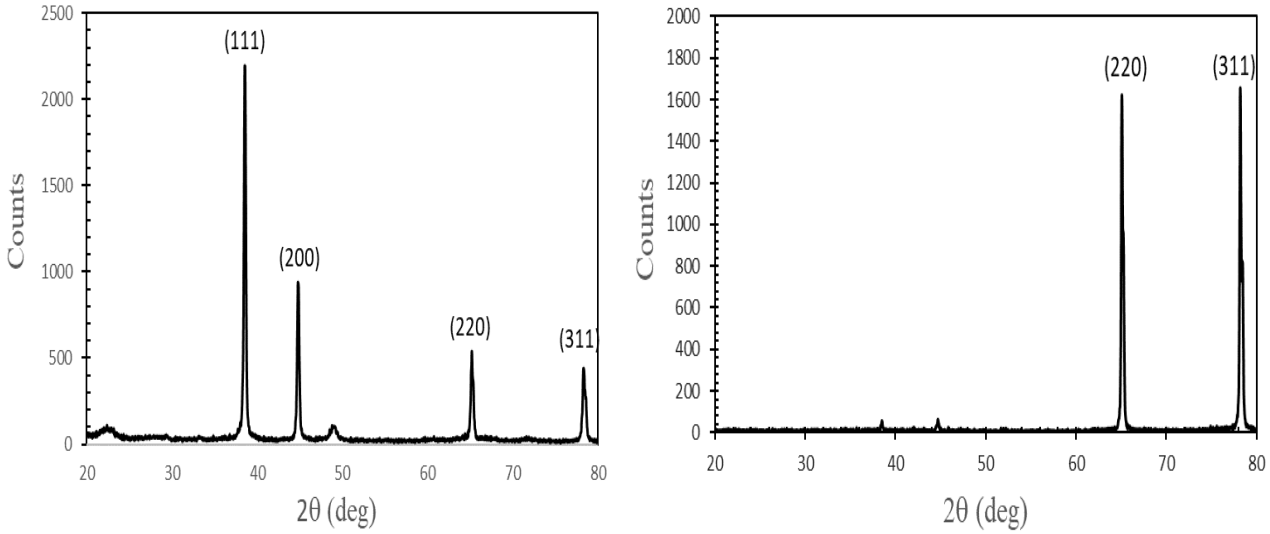

Figure 3: (a) The XRD patterns of Al NPs. (b): XRD patterns of Aluminum bulk.

Table 1: X-ray diffraction peaks of Al NPs. The data are approximated to three significant figures.

Peak No.	2Θ (deg.)	Miller indices	β=FWHM (deg)	D (nm)	$\delta=1/D^2$ (cm^{-2})
1	38.5	(111)	0.240	35.1	8.125
2	44.5	(200)	0.238	36.1	7.659
3	65.2	(220)	0.254	37.1	7.267
4	78.4	(311)	0.268	38.2	6.843

Table 2: X-ray diffraction peaks of Al bulk.

Peak No.	2Θ (deg.)	Miller indices	β=FWHM (deg)	D (nm)	$\delta=1/D^2$ (cm^{-2})
1	65.08	(220)	0.192	49.1	4.147
2	78.20	(311)	0.203	50.6	3.904

4.2. Scanning Electronic Microscopy

The surface morphology and size of the aluminum have been analyzed by SEM, which is used for more detailed morphological studies. Figure 4a manifests the SEM image for Al NPs with a scale bar of 200 nm. The particles have spherical-like shapes with a rather uniform size. Image-J program has been used to calculate the average particle size of Al NPs, which is about 145 nm. Figure 4b displays a SEM micrograph of pure Al bulk. This Figure clearly illustrates that the particles also have spherical-like shapes but they have a tendency to agglomerate and the average particle size is about 75 nm.

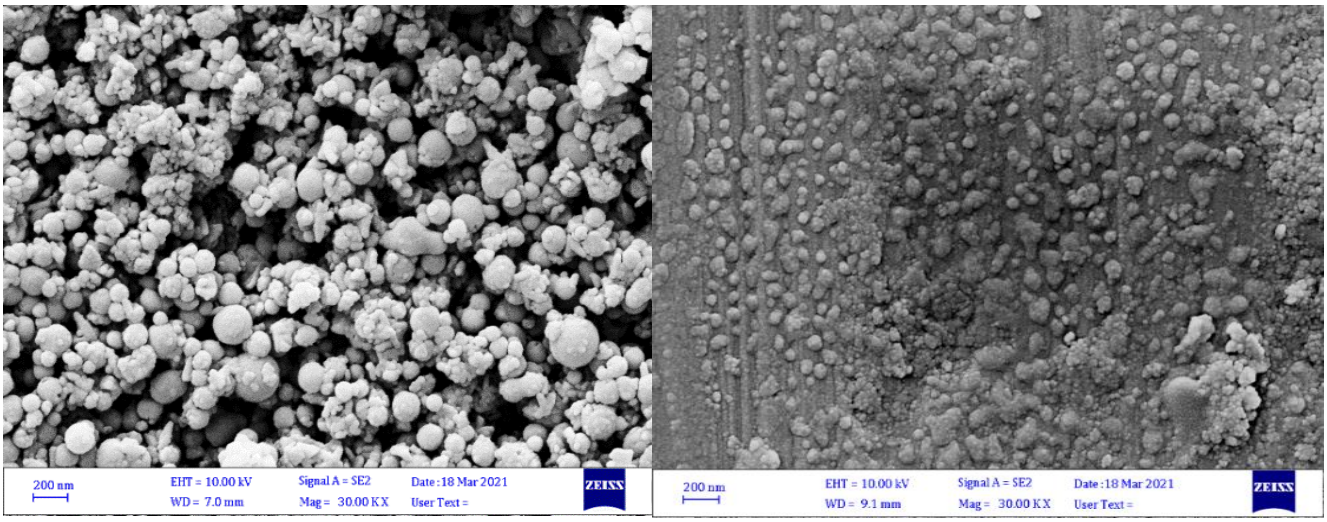

(a) **(b)**

Figure 4: (a) Scanning electron micrographs of Al NPs (scale bar 200 nm). (b) Scanning electron micrographs of Al bulk (scale bar 200 nm).

4.3 Plasma Emission Analysis

4.3.1. Emission Spectrum of Aluminum Plasma

The emission spectra of Al NPs and Al plasma are elucidated in Figures 5 and 6, correspondingly. The emission spectra of the Al plasma created by laser was recorded using energy (400-700 mJ). The emission spectrum of the Al plasma produced was recorded in the visible region by the spectroscopy (250-700 nm). This spectrum exhibits the atomic emission intensity for aluminum Al I at wavelengths of 257.51, 305.71, 309.27, 349.40 and 396.15 nm. The ionic emission intensity for aluminum Al II also appears at wavelengths of 281.62, 358.66, 466.68, 559.33, and 620.15 nm. There are other peaks at 388.91, 410.17, 486.14, and 656.28 nm, which correspond to the H line for hydrogen atoms. Since the rate of the mass ablation of the target raises with the increase of the pulse laser energy, the intensity of the whole emission lines also rises. As the laser energy increases, its plasma absorption rises, ensuing an increased ablation and an increase in the intensity of plasma emission spectral lines. According to the results shown in Figure 5 and 6, it was found that the whole intensity of the Al I emission line is considerably greater than that for Al II. This result is in agreement with Pakhal [30].

Table 3 lists the calculated electron temperature (T_e), electron density (n_e), plasma frequency (f_p) and Debye length (λ_D) for Al NPs as well as Al bulk target at different laser pulse energies (400 to 700 mJ) by using the Boltzman and Stark broadening. Because f_p is proportional to n_e, it indicates that f_p raises as the laser energy increases, but λ_D decreases.

Table 3: Plasma parameters for Al NPs and Al bulk with different laser energy.

Aluminum Samples	E (mJ)	T_e (eV)	FWHM (nm)	n_e*10^{16} (cm^{-3})	f_p*10^{12} (Hz)	λ_D*10^{-6} (cm)
Al NPs	400	0.520	1.800	57.382	6.802	0.707
	500	0.570	1.900	62.133	7.078	0.712
	600	0.644	2.000	67.004	7.351	0.728
	700	0.645	2.000	67.004	7.351	0.729
Al bulk	400	0.516	1.500	43.880	5.949	0.805
	500	0.568	1.600	48.251	6.238	0.806
	600	0.582	1.700	52.753	6.522	0.780
	700	0.592	1.750	55.052	6.663	0.771

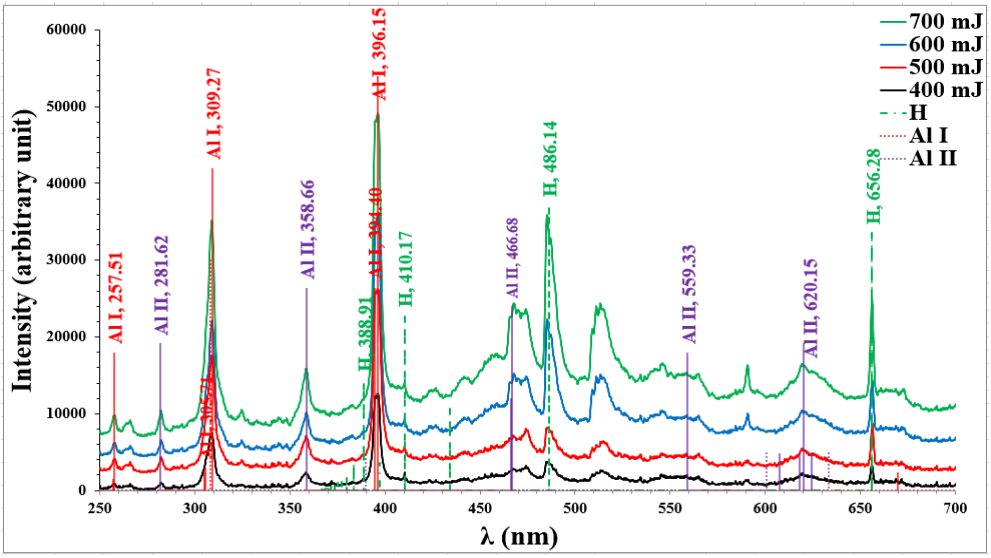

Figure 5: The emission spectra of the laser-induced Al NPs target with various laser energies (400, 500, 600, and 700 mJ).

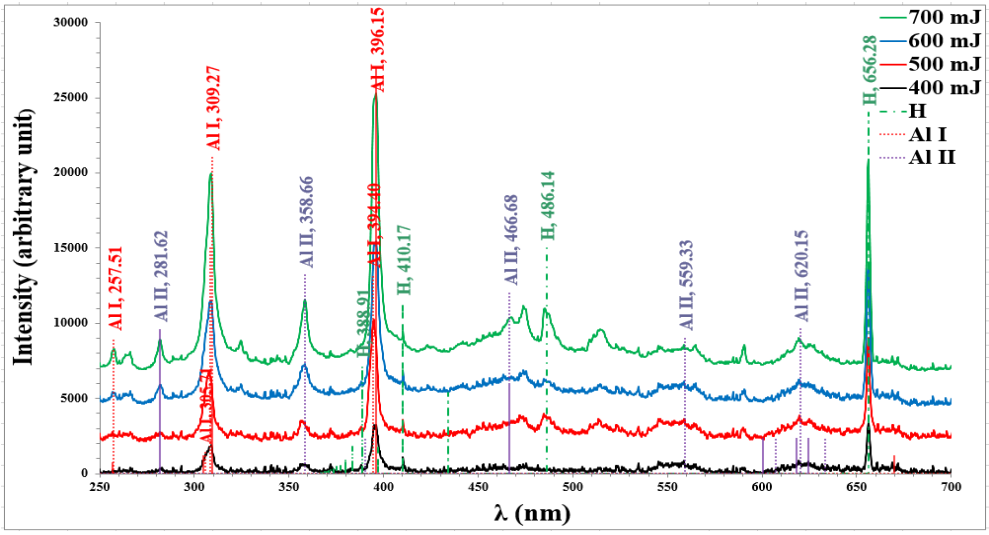

Figure 6: Emission spectra of the laser-induced Al bulk target with laser energies of 400, 500, 600, and 700 mJ.

4.3.2. Influence of Al Metal on the Electron Temperature

Eq. (3) can be used to calculate the electron temperature (T_e) of plasma for Al bulk and Al NPs. The electron temperature was obtained using the atomic lines of the Al NPs(I) and Al(I) elements at various laser intensities (400, 500, 600 and 700 mJ). Electron temperature can be found using NIST data [25] and Eq. (3). Figure 7 reveals the electron temperature change with the laser energy in the Al NPs and Al bulk plasma. Under the same conditions, the electron temperature in the Al NPs plasma is greater than that for the Al bulk plasma.

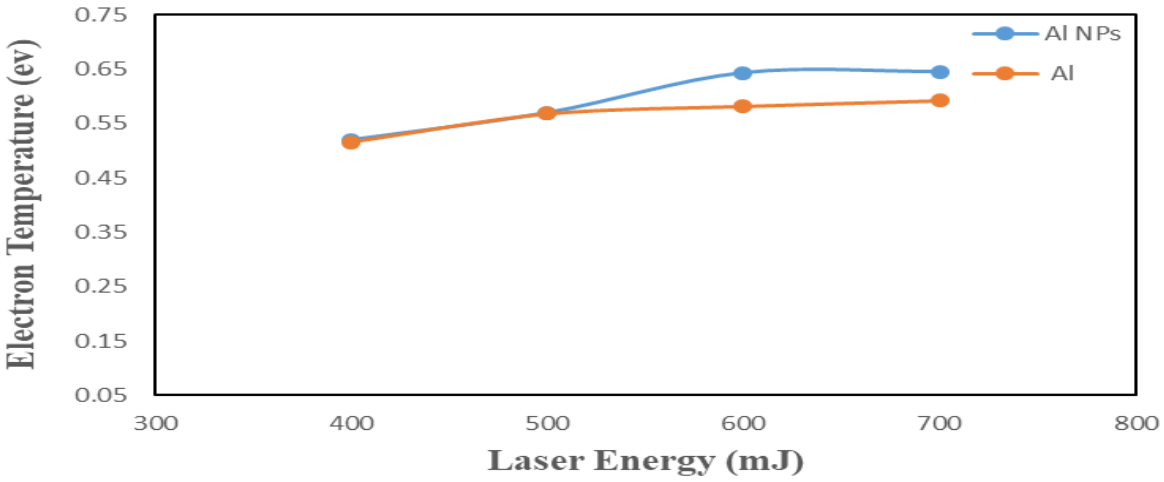

Figure 7: The variation of electron temperature with laser energy in Al bulk and Al NPs plasma at atmospheric pressure.

4.3.3. Influence of Al Metal on the Electron Density

The effect of laser energy on the electron density of Al as a bulk and as a nanoparticles is studied using Eq. (2) and NIST data [25]. Figure 8 shows that the electron density of both plasmas is directly proportional to the laser energy. At similar laser energies, the electron density of plasma for Al NPs is higher than that of plasma generated from Al in its bulk form.

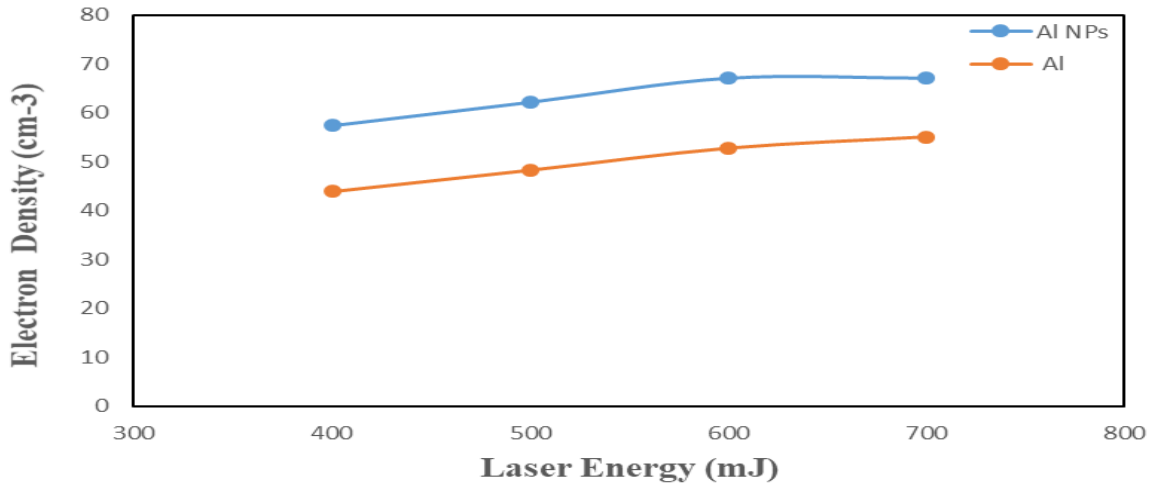

Figure 8: The electron density change with the laser energy of Al bulk and Al NPs plasma at the atmospheric pressure.

4.3.4. Effect of Laser Energy on the Plasma Frequency

Figure 9 depicts the differences in electron frequency with the laser energy for plasmas generated from Al bulk and Al NPs. The data points in the graph showed that the plasma frequency increased as the laser energy increased for both plasmas. The increase in plasma frequency is a result of the increased concentration of electrons which is a function of laser energy. According to this explanation, the plasma frequency in the Al NPs plasma is greater than in the Al bulk plasma.

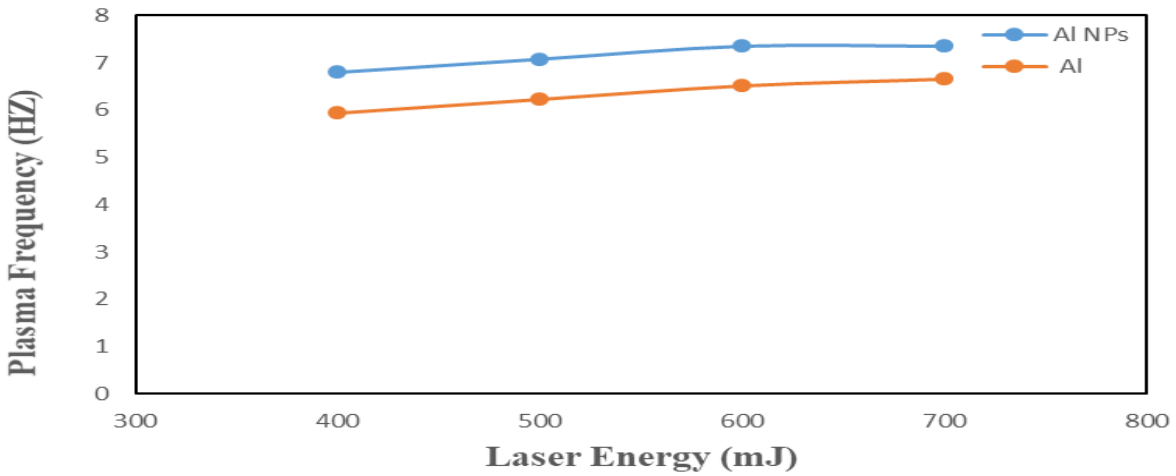

Figure 9: The variation of plasma frequency with laser energy for Al bulk and Al NPs plasma at the atmospheric pressure.

5. Conclusions

In this article, the results showed that the electron temperature in the plasma in increases with increased laser energy. The plasma temperature formed by the nano aluminum target is higher than that of the plasma formed by the bulk aluminum target at identical laser energy. Furthermore, as the radiance of the laser increases, more interesting species, like the ions and as well as free electrons, are produced. High electron density generated from nano aluminum plasma compared with that generated from the Al bulk target. The differences between the plasma spectrum for the two forms of alumium can be attributed to the differences in their topographical structures.

Acknowledgement

We would like to thank the University of Baghdad and the Physical Science Department in Baghdad, Iraq, for their assistance in conducting this study.

Conflict of Interest

The researchers of this paper state that they possess no conflict of interest.

References

[1] D. M. Wong, A. A. Bol'shakov, and R. E. Russo, "Laser Induced Breakdown Spectroscopy," 3nd ed., *Encyclopedia of Spectroscopy and Spectrometry*, 2016.

[2] A. K. Patnaik, Y. Wu, P. S. Hsu, M. Gragston, Z. Zhang, J. R. Gord, *et al.*, "Simultaneous LIBS Signal and Plasma Density Measurement for Quantitative Insight Into Signal Instability at Elevated Pressure," *Optics Express*, vol. 26, p. 25750, 2018.

[3] G. S. Maurya, A. Marín-Roldán, P. Veis, A. K. Pathak, *et al.*, "A Review of the LIBS Analysis for the Plasma-Facing Components Diagnostics," *Journal of Nuclear Materials*, vol. 541, p. 1-54, 2020.

[4] N. M. Saadoon, N. M. Hadi, and S. H. Sabeeh, "Diagnosis of Copper Plasma by Laser Induced Breakdown Spectroscopy," IOP Conference Series: Materials Science and Engineering, vol. 757, p. 012023, 2020.

[5] A. M. Popov, F. Colao, and R. Fantoni, "Enhancement of LIBS Signal by Spatially Confining the Laser-Induced Plasma," *Journal of Analytical Atomic Spectrometry*, vol. 24, p. 602–604, 2009.

[6] F. B. Gonzaga and C. Pasquini, "A Compact and Low Cost Laser Induced Breakdown Spectroscopic System: Application for Simultaneous Determination of Chromium and Nickel in Steel using Multivariate Calibration," *Spectrochimica Acta Part B*, vol. 69, p. 20–24, 2012.

[7] J. Yu and R. Zheng, "Laser-Induced Plasma and Laser-Induced Breakdown Spectroscopy (LIBS) in China: The Challenge and the Opportunity," *Frontiers of Physics*, vol. 7, p. 647–648, 2012.

[8] V. Lednev, S. M. Pershin, and A. F. Bunkin, "Laser Beam Profile Influence on LIBS Analytical Capabilities: Single vs. Multimode Beam," *Journal of Analytical Atomic Spectrometry*, vol. 25, p. 1745–1757, 2010.

[9] S. M. Aberkane, A. Bendib, K. Yahiaoui, S. Boudjemai, S. Abdelli-Messaci, T. Kerdja, *et al.*, "Correlation Between Fe-V-C Alloys Surface Hardness and Plasma Temperature via LIBS Technique," *Applied Surface Science*, vol. 301, p. 225–229, 2014.

[10] S. H. Ahmadi, M. H. Keshavarz, and H. R. Hafizi Atabak, "Introducing Laser Induced Breakdown Spectroscopy (LIBS) as a Novel, Cheap and Non-destructive Method to Study the Changes of Mechanical Properties of Plastic Bonded Explosives (PBX)," *Journal of Inorganic and General Chemistry*, vol. 644, p. 1667–1673, 2018.

[11] Q. Wang, A. Chen, D. Zhang, Y. Wang, L. Sui, S. Li, *et al.*, "The Role of Cavity Shape on Spatially Confined Laser-Induced Breakdown Spectroscopy," *Physics of Plasmas*, vol. 25, p. 1–7, 2018.

[12] Y. A. Ali and R. A. Khamis, "Spectroscopic Study of Copper Plasma Produced by Nd: YAG Laser from The Nano and Bulk Copper Targets," Journal of Physics: Conference Series, vol. 1818, p. 012008, 2020.

[13] X. Xu, C. Du, F. Ma, Y. Shen, *et al.*, "Fast and Simultaneous Determination of Soil Properties using Laser-Induced Breakdown Spectroscopy (Libs): A Case Study of Typical Farmland Soils in China," *Soil Systems*, vol. 3, p. 1–18, 2019.

[14] A. Khumaeni, T. Motonobu, A. Katsuaki, M. Masabumi, *et al.*, "Enhancement of LIBS Emission using Antenna-Coupled Microwave," *Optics Express* vol. 21, p. 29755, 2013.

[15] A. k. AL-Ogaili, A. K. Ali, and T. H. Ali, "Preparation of Silver Nanoparticles and Study the Optical and Antibacterial Properties," *Engineering and Technology Journal*, vol. 33, p. 478–487, 2015.

[16] A. S. Jawad, Q. N. O. Thewaini, and S. Al-Musawi, "Cytotoxicity Effect and Antibacterial Activity of Al2O3 Nanoparticles Activity against Streptococcus Pyogenes and Proteus Vulgaris," Journal of Applied Sciences and Nanotechnology, vol. 1, p. 42-50, 2021.

[17] M. Al-Kinani, A. Haider, and S. Al-Musawi, "Study the Effect of Laser Wavelength on Polymeric Metallic Nanocarrier Synthesis for Curcumin Delivery in Prostate Cancer Therapy: In Vitro Study," *Journal of Applied Sciences and Nanotechnology*, vol. 1, p. 43–50, 2021.

[18] S. Z. Al Sheheri, Z. M. Al-Amshany, Q. A. Al Sulami, N. Y. Tashkandi, *et al.*, "The Preparation of Carbon Nanofillers and their Role on the Performance of Variable Polymer Nanocomposites," *Designed Monomers and Polymers.*, vol. 22, p. 8–53, 2019.

[19] S. A. M. Mansour, "Self-Absorption effects on electron temperature-measurements utilizing laser induced breakdown spectroscopy (LIBS)-techniques," *Optics and Photonics Journal*, vol. 05, no. 03, pp. 79–90, 2015.

[20] M. Fikry, W. Tawfik, and M. Omar, "Measurement of the Electron Temperature in a Metallic Copper Using Ultrafast Laser-Induced Breakdown Spectroscopy," *Journal of Russian Laser Research*, vol. 41, p. 484–490, 2020.

[21] M. A. Khalaf and W. J. Hmood, "Influence of Laser Energies on Tin Oxide Nanoparticles Plasma Parameters Prepared by Nd: YAG Laser," *The Scientific Journal of King Faisal University*, vol. 21, p. 401-406, 2020.

[22] T. Hussain, M. A. Gondal, and M. Shamraiz, "Determination of Plasma Temperature and Electron Density of Iron in Iron Slag Samples using Laser Induced Breakdown Spectroscopy," *IOP Conference Series: Materials Science and Engineering*, vol. 146, p. 012017, 2016.

[23] A. Latif, K. A. Bhatti, M. S. Rafique, *et al.*, "Investigations on Laser Induced Nickel and Titanium Plasmas," *Pakistan Journal of Engineering and Applied Sciences*, vol. 9, p. 28–33, 2011.

[24] M. Mathuthu, R. M. Raseleka, A. Forbes, *et al.*, "Radial Variation of Refractive Index, Plasma Frequency and Phase Velocity in Laser Induced Air Plasma," *IEEE transactions on plasma science*, vol. 34, p. 2554–

2560, 2006.

[25] “Atomic Spectra Database | NIST.” https://www.nist.gov/pml/atomic-spectra-database (Accessed Sept. 14, 2021).

[26] R. Huseen, A. Taha, and O. Abdulhusein, "Study of Biological Activities of Magnetic Iron Oxide Nanoparticles Prepared by Co-Precipitation Method," *Journal of Applied Sciences and Nanotechnology*, vol. 1, p. 37–48, 2021.

[27] K. S. Khashan, G. M. Sulaiman, F. A. Abdulameer, S. Albukhaty, M. A. Ibrahem, T. Al-Muhimeed, and A. A. AlObaid. "Antibacterial Activity of TiO2 Nanoparticles Prepared by One-Step Laser Ablation in Liquid," *Applied Sciences*, vol. 11, p. 4623, 2021.

[28] R. S. Tabari, M. Halali, A. A. Javadi, and M. H. Khanjanpour, "Experimental Analysis and Characterization of High-Purity Aluminum Nanoparticles (Al-Nps) by Electromagnetic Levitation Gas Condensation (ELGC)," *Nanomaterials*, vol. 10, p. 1–15, 2020.

[29] Suprapedi, Mulyadi, P. Sardjono, and Ramlan, "Preparation and Characterization of Alloy Al -SiC Made by Using Powder Metallurgy Method," *AIP Conference Proceedings*, vol. 2221, p. 5–11, 2020.

[30] H. R. Pakhal, R. P. Lucht, and N. M. Laurendeau, "Spectral Measurements of Incipient Plasma Temperature and Electron Number Density During Laser Ablation of Aluminum in Air," *Applied Physics B*, vol. 90, p. 15–27, 2008.